ADVANCED PHOTONICS RESEARCH
Open Access
www.adpr-journal.com

Localized Surface Plasmon Resonance Optical Biosensor for Simple Detection of Deoxyribonucleic Acid Mismatches

Masixole Yvonne Lugongolo, Saturnin Ombinda-Lemboumba, Lerato Hlekelele, Nontsikelelo Nyokana, and Patience Mthunzi-Kufa*

Optical biosensors are optical technologies that evaluate changes in the refractive index as they monitor non-covalent molecular interactions in real time. These make use of unsophisticated, label-free analytical approaches, which do not require dyes to produce a visible signal. In this study, the efficiency of localized surface plasmon resonance (LSPR) biosensor in detecting a single nucleotide mismatch in deoxyribonucleic acid is examined. The detection is based on the hybridization of a target DNA at 100 ng μL^{-1} with a complementary biotinylated probe as well as a partially complementary biotinylated with one nucleotide mismatch probe on a gold-coated surface. Both probes are used at a concentration of 0.1 μm. The LSPR exhibited sensitivity by differentiating sample M+ from sample C+ through varying transmission intensities of 0.28 and 0.26 μA, respectively. Based on these findings, this approach demonstrates a great potential due to its ability to distinguish samples that differ with a single base pair, and its efficiency will be explored in the development of a point-of-care device as a simpler and cost-effective approach for detection of various biologically and medically significant mutations such as antimicrobial resistance mutations. More work is underway to determine the robustness of the LSPR biosensor using the biotin–neutravidin approach.

1. Introduction

Deoxyribonucleic acid (DNA) is a complex, long biological molecule; present within every cell in most living organisms; and carries all the information essential to make and sustain an organism.[1] It is typically composed of two polynucleotide chains that due to twisting around each other form a double-helix molecule.[2] Each strand is a long sequence of nucleotides made of a deoxyribose sugar, a phosphate group as well as one of four nitrogen-containing nucleobases, which are cytosine [C], guanine [G], adenine [A], or thymine [T].[3] The double-stranded form of DNA is due to base pairing between nucleotides, where A pairs with T, and G pairs with C. Precisely, adenine and thymine are complementary base pairs, and cytosine and guanine are also complementary base pairs. As such, according to Chargaff's rule, because of their complementarity, there is as much adenine as thymine in a DNA molecule and as much guanine as cytosine.[3] Adenine and thymine are linked by two hydrogen bonds, and cytosine and guanine are linked by three hydrogen bonds. The two strands are antiparallel, which means that one strand will have the 3' carbon of the sugar in the "upward" position, whereas the other strand will have the 5' carbon in the upward position. The diameter of the DNA double helix is the same all over because a purine, which has two rings always pairs with a pyrimidine that contains only one ring and their collective lengths are always identical.[3] The specific base pairing allows for DNA duplication during mitosis and cell growth.[4]

However, during DNA replication, errors sometimes occur leading to base pair mismatch, which can remain uncorrected despite the DNA undergoing DNA repair processes, whereby repair enzymes recognize the flaws between inappropriately paired nucleotides. This unfortunate event alters the genetic

M. Y. Lugongolo, S. Ombinda-Lemboumba, P. Mthunzi-Kufa
Photonics Centre
Council for Scientific and Industrial Research
PO Box 395, Pretoria 0001, South Africa
E-mail: mlugongolo@csir.co.za

L. Hlekelele, N. Nyokana
Centre for Nanostructures and Advanced Materials
DSI-CSIR Nanotechnology Innovation Centre
Council for Scientific and Industrial Research
Pretoria 0001, South Africa

P. Mthunzi-Kufa
School of Chemistry and Physics
University of KwaZulu-Natal
Pietermaritzburg Campus, King Edward Avenue, Pietermaritzburg 3201, South Africa

P. Mthunzi-Kufa
Department of Human Biology
Division of Biomedical Engineering
University of Cape Town
Cape Town 7925, South Africa

The ORCID identification number(s) for the author(s) of this article can be found under https://doi.org/10.1002/adpr.202300283.

DOI: 10.1002/adpr.202300283

information, a phenomenon commonly known as mutation.[5] Changes in gene's DNA can have either beneficial or harmful effects.[6,7] Positive mutations improve the fitness of an organism since they generate new protein versions that enable an organism to adapt to changes in their environment. Mutations like the ones that occur in bacteria thereby allowing them to survive in the presence of antibiotics. Such mutations have given rise to antibiotic-resistant strains of bacteria, which benefits the organism and yet they are a public health concern.[8] Another positive mutation is the C–C chemokine receptor type 5 (CCR5)-delta 32 mutation, which hinders human immunodeficiency virus' (HIV) ability to enter the immune cells. The CCR5 co-receptors aids HIV entry into cells, the delta 32 mutation causes the CCR5 to be smaller than usual and cannot be expressed on the cell surface, thus preventing HIV infection.[9] Mutations are likely to result in malfunctioning proteins as well as defective proteins that do not function at all. Such mutations are likely to be harmful as a result cause genetic defects or cancer.[6,7] An example of such a genetic defect is cystic fibrosis, which causes the body to create thick, slimy mucus that blocks the lungs and ducts in digestive organs.[10] Numerous detection methods, including oligonucleotide ligation, allele-specific primer extension, and allele-specific hybridization are available, and they used to identify various kinds of mutations.[11,12] However, these techniques are hindered by complex processes and instrumentation that make it difficult to perform mutation detection experiments in resource-limited settings. Hence, the current study focuses on examining the efficiency of localized surface plasmon resonance (LSPR) biosensor in detecting DNA mismatches for the development of an optics-based point-of-care device for use in resource-limited settings, as there is an increasing need to discover ways to make simpler diagnostic approaches that do not compromise patient care quality.[13] Point-of-care diagnostics devices do not require trained laboratory staff and sophisticated facilities to run tests and obtain results.[14] The approach investigated in this study will lead to the development of a device that can detect various genetic mutations including drug resistance mutations that render some antimicrobial drugs ineffective such as what has been observed in HIV and tuberculosis treatments.[15,16]

Optical biosensors are small analytical tools with biorecognition elements integrated to optical transducer systems such as surface plasmon resonance (SPR), LSPR, interferometers, refractometers, and gratings.[17,18] They are simple devices with a primary objective of producing a signal which is proportional to the analyte concentration as well as the binding strength between the analyte and biorecognition element.[18] They use antigens, antibodies, enzymes, proteins, receptors, and nucleic acids as biorecognition elements.[19] Optical biosensors are more advantageous than conventional devices because they can provide label-free, direct, and real-time detection of various materials of interest. Additionally, optical biosensors are cost-effective, small, highly sensitive, and specific.[17,19] They make use of the evanescent phenomenon in which waves are generated when light hits a metal film. The most common optical biosensors are the SPR and LSPR biosensors.[17] The LSPR takes place when incident light interacts with metallic nanoparticles, typically gold and silver. The electromagnetic field of the light induces collective electron charge oscillations confined in metallic nanostructures followed by the absorbance of light within the ultraviolet–visible (UV–vis) band.[20] LSPR is different from SPR since the plasmons oscillate locally rather than along the metal–dielectric interface. Thus, the decay length of the electromagnetic field observed is greater in SPR in the range of 200 nm, while it is less in LSPR in the range of 6 nm.[21,22] The LSPR's shorter field decay length offers increased sensitivity to refractive index changes on the surface.[17] Furthermore, LSPR biosensors are biocompatible, and offer real-time monitoring of various analytes with strong stability and label-free detection, qualities that provide a foundation for biosensing applications.[23] The proficiency of LSPR biosensors has been examined in various fields. In food quality and safety, these biosensors have been employed for the detection of microbial agents such as bacteria and viruses.[24–27] Similarly, in medical diagnostics, it is utilized for the analysis of medical specimens such as serum, urine, blood, mucous, and sputum for the presence disease causing agents.[28–31] In another study, LSPR - based metal nanodiscs were employed for the rapid detection of severe acute respiratory syndrome coronavirus 2 (SARS-CoV-2).[32] These biosensors have been used to detect protein – protein interactions, a phenomenon that plays a pivotal role in various biological processes as proteins operate in complexes and the analysis of their interactions enables understanding of cellular organizations.[33,34] LSPR sensors have been employed for nucleic - acid-related studies, by detecting DNA and monitoring interactions of DNA and enzymes.[35,36] Rapisarda successfully developed a single nucleotide mismatch detection method based on the DNA -hybridization process. Their approach demonstrated high specificity and sensitivity.[37] In another study, LSPR biosensing was developed to detect p53 mutations.[38] It has also been used in more advanced applications such as multiplexing applications as well as integration of LSPR with microfluidics. Chen et al. developed a multiplex – microfluidic device for the detection of inflammatory biomarkers such as IgG, tumour necrosis factor alpha, and C-reactive protein.[39] However, in terms of refractive index sensitivity, LSPR is less sensitive in comparison the SPR.[40] Sometimes, LSPR sensing devices have great regions of dielectric materials, which might stimulate the adsorption of the analyte. Such regions need to be obstructed to maintain the accuracy of measurements.[41] Some of the studies that have used LSPR for nucleic acid mismatch detection employ various approaches, which all seem to have a potential of contributing toward the generation of a simple - to - use tool.[42–46]

Biomolecules such as DNA, ribonucleic acid (RNA), proteins, and antibodies are immobilized onto the metal surface. A change in the refractive index of the biomolecules immobilized on the metal surface results in a change of the transmitted intensity.[47] The plasmons are responsive to the metal surface environment. As such, any changes that take place at the surface affect how light is absorbed and cause transmitted intensity changes.[48] Hence, when an analyte binds to the immobilized molecule at the metal surface causes changes in the signal; allowing interactions to be measured without labels.[47,48] The aim of this study was to examine the efficiency of LSPR biosensor in detecting a single nucleotide mismatch in DNA. This was done by sequencing a small region with a plasmid DNA before designing probes. After confirming the target region sequence, probes were designed and synthesized. Thereafter, DNA-hybridization

experiments were performed on a gold-coated surface and analyzed on the LSPR optical biosensing system.

2. Methodology

2.1. Sequencing of the Target DNA

A 1320 base pair (bp) region of the HIV *pol* gene within pSG3Δ*env* vector was used as a target region for this study and it was sequenced using the following primers: forward primer 5' tacaatgtgcttccacaggg 3' and reverse 5' tggctactatttcttttgct 3' at Inqaba Biotech (Pretoria, South Africa).

2.2. Polymerase Chain Reaction

A polymerase chain reaction (PCR) to amplify the 1320 bp region as well as a 174 bp region within the 1320 bp was carried out using Axygen MaxyGene thermal cycler (Corning, New York, US) with Invitrogen Platinum SuperFi II PCR Master mix (ThermoFisher Scientific, Massachusetts, US). The 1320 bp nucleotide region was amplified using the same primers used in the sequencing experiment, while the 174 bp region (sequence of interest) was amplified using the following primers: forward primer: 5' ggtggggatttaccacacca 3' and reverse primer: 5' gacttgcccaattcaatttt 3'. The PCR reactions were performed in a total volume of 50 μL backbone vector DNA, forward primer, reverse primer, and platinum SuperFi II PCR Master Mix (Invitrogen, Waltham, Massachusetts, US). The cycling conditions consisted of an initial denaturation at 98 °C for 30 s, and then 35 cycles of 98 °C for 10 s, 60 °C for 10 s, and 72 °C for 30 s. In the final cycle, extension conducted at 72 °C for 5 min. Amplification products of DNA were confirmed using gel electrophoresis in 2% agarose gels containing ethidium bromide and detected by GelDoc-It Imager.

2.3. Probe Design

The two 5'-biotinylated probes used in this work were designed according to the target sequence and synthesized at Inqaba Biotech. The first probe was 100% complementary (Probe C) to the underlined region of the target sequence (ctttcttggaggtaaggaaaccta) and the second probe was also complementary (probe M) with a single nucleotide mismatch (ctttcttgaaggtaaggaaaccta). The mismatched nucleotide is in red text.

2.4. DNA Hybridization

A gold-coated slide was created by depositing a 40 nm gold film on a glass slide thinly coated with a 5 nm layer of titanium to enhance gold binding on glass using the HEX benchtop thin-film deposition system (Korvus Technology Ltd., UK).[49] Following the coating of glass slides with gold, the slides we re characterized using scanning electron microscopy to evaluate the surface of the sensor slide.[50] The gold-coated sensor slide was washed in acetone followed by ethanol and ultrapure water and dried under nitrogen gas. The slide was then immersed in 1 mM 11-mercaptoundecanoic acid (Sigma Aldrich, St. Louis, Missouri, US) and incubated for 2 h at room temperature in the dark. After 2 h incubation, the slide was rinsed with 1X phosphate-buffered saline (PBS) (ThermoFisher Scientific, Massachusetts, US) and activated by soaking for 10 min in 1-ethyl-3-(3-dimethylaminopropyl)carbodiimide/N-hydroxysuccinimide (EDC/NHS) (Sigma Aldrich, St. Louis, Missouri, US) at the concentrations of 5 and 13 mM, respectively. The EDC/NHS-activated slide was rinsed before adding 6 μL of 0.2 mg mL^{-1} neutravidin in all wells. The wells were created by pasting ring stickers on the activated slide. In total, there were 5 wells $samples^{-1}$ as summarized in **Table 1**. After an hour of incubation with neutravidin (ThermoFisher Scientific, Massachusetts, US), the excess neutravidin was rinsed out with 1X PBS prior to adding 6 μL of 0.1 μM biotinylated probes in samples C–, C+, M–, and M+. The samples were incubated for 1 h. Following the rinsing of wells with PBS and 6 μL of 100 ng μL^{-1}, target DNA was then added in samples C+ and M+ before incubating for 30 min. The unbound DNA was rinsed out before analyzing the samples on the LSPR setup. The volume of the reagents added in the wells was influenced by the size of the well. The wells used in the study were 5 m m in diameter and 3 μL was sufficient to cover the entire surface of the well ; however , 6 μL was used to overfill the wells.

2.5. LSPR Detection

The LSPR setup (as outlined in **Figure 1**) used in this work was a home-built system that consisted of a 627 nm light-emitting diode (LED) with a total power output of 5.8 mW as the light source. The light from the LED was used to illuminate the metal surface with the immobilized biomolecule (biosensor chip). The light emanating from the biosensor chip was directed to photodiode detector. The photodiode was connected to photodiode signal amplifier system to monitor the small intensity variation on the biosensor chip surface and enhance the strength of the photodiode signal. The values of the transmitted intensity were then recorded. Of note, the photodiode signal was converted to current by the photodiode amplifier system and the readout was displayed in microampere.

2.6. Bioconjugation of DNA to Gold Nanoparticles

In this experiment, 90 nm streptavidin-functionalized gold nanoparticles (AuNPs) from cytodiagnostics (Burlington, Canada) were used. Samples were named in the same way as provided in Section 2.4 and Table 1. They were prepared in the following manner: in the reference sample, the nanoparticles were mixed with 1X PBS, while samples C–, C+, M–, and M+ were prepared

Table 1. Constituents of each well/sample in DNA-hybridization experiments.

Samples	Components of the wells
Sample R	Reference sample (functionalized gold surface with no DNA)
Sample C–	Complementary probe
Sample C+	Complementary probe with target DNA
Sample M–	Mismatch probe
Sample M+	Mismatch probe with target DNA

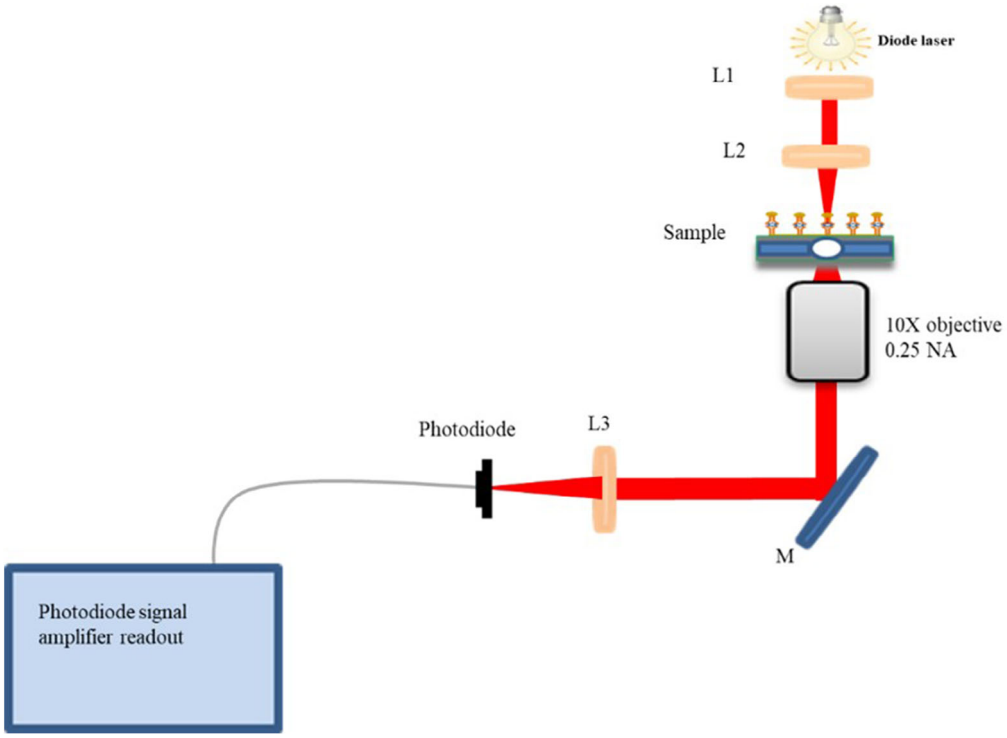

Figure 1. Localized surface plasmon resonance setup.

by mixing AuNPs with the biotinylated probes and incubated for 30 min at room temperature in the dark. The mixtures were then centrifuged at 14000 g for 30 min at 23 °C. The supernatant was removed, and the target DNA was added to samples C+ and M+. The samples were incubated for 30 min at room temperature in the dark and they were later centrifuged at14000 g for 30 min. The samples were characterized by UV–vis spectroscopy, Fourier-transform infrared spectroscopy (FTIR), zeta potential, dynamic light scattering (DLS), and transmission electron microscopy (TEM).

2.7. Statistics

The experiments were repeated three times and an average of the data obtained was used to plot the graph. Sample R was used as a reference. Using Microsoft Excel, the mean and standard deviation were calculated. A t test was used to find the statistical difference between the experimental groups and reference. The results were deemed significantly different at $p < 0.05$ using at test.

3. Results and Discussion

The sequence of the target region was confirmed by DNA sequencing. The sequencing results were compared and aligned with other HIV-1 sequences on BLAST.[51] The results demonstrated that the region of interest in the pSG3Δenv vector was 98% like the sequences available in literature as shown in **Figure 2**.[52] The top sequence is the pSG3Δenv vector sequence and the bottom one is the reference sequence on blast. The blue highlighted area is a 174 bp region that was used for the experiments conducted in this work.

The similarities between the sequences are represented by the small lines between the vector and the reference sequence. Therefore, the absence of the lines between the sequences indicates that there were no similarities between the sequences at that nucleotide base.

The 1320 bp region sequenced was PCR amplified as shown by the 1320 bp band in lane 3 of **Figure 3** and the 174 bp DNA sequence used in the study was also amplified as exhibited by a band in lane 2 of Figure 2. In contrast, lane 1 contains a middle range DNA ladder with bands from 100 to 5000 bp. DNA agarose gel electrophoresis confirmed that the two amplicons; 174 and 1320 bp were the expected sizes indicating that the primers successfully bound to the target regions.

Having confirmed by PCR and gel electrophoresis that the region of interest was present, the 174 bp amplicon was used as a target sequence for DNA-hybridization experiments analyzed on the LSPR optical setup and in AuNPs bioconjugation experiments for UV–vis spectroscopy, FTIR, TEM, DLS, and zeta potential analysis.

Since the aim of this study was to investigate the efficiency of LSPR optical biosensor in detecting DNA mismatches, DNA-hybridization experiments were analyzed on the LSPR system described in Section 2.4, Figure 1. The biotinylated probes were immobilized onto a surface that had been functionalized with neutravidin because of the strong interaction between biotin and avidin. The avidin–biotin bond is one of the known strongest non-covalent interactions involving a protein and a ligand.

Figure 2. Sequencing results showing similarities between the vector sequence (top) and the reference sequence (bottom). The similarities are represented by the small lines between the two sequences. The blue highlighted section is the region of interest.[52]

The bond formation between biotin and avidin is quick, and once it is established, it cannot be affected even by significant changes in pH, temperature, and other conditions that would normally affect some molecule-to-molecule interaction.[53] Immobilization of biotinylated molecules on avidin-coated surface is an extensively used approach that is generally recommended for the binding of nucleic acids because it allows the orientation of the probe to be preserved.[54] **Figure 4** shows the results obtained indicating the light-transmitted intensity of different samples, with sample R exhibiting the highest intensity of transmitted light of 0.32 μA among all the samples. When comparing sample R with sample C–, M–, and M+, there is a significant difference of $p < 0.05$ of the transmitted light and a difference of $p < 0.01$ when compared to sample C+.[55,56]

All the other samples contained DNA and the distinguishable levels of transmitted light intensity could be attributed to the absence of DNA in sample R, thereby affecting the refractive index (n) of that sample since ssDNA monolayer has a refractive index of 1.46.[30] The addition of DNA on samples increases the value of the refractive index, thus changing the amount of light transmitted. Furthermore, it was observed that samples C− and M− had similar levels of transmitted light intensities of 0.29 μA. This was expected because both probes bind to the avidin-coated surface in the same way and they are very similar to each other as

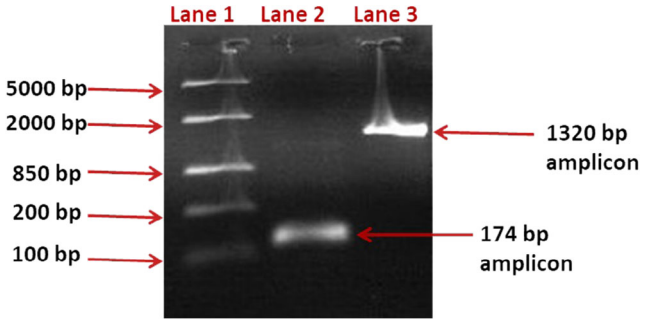

Figure 3. PCR amplification of the target region: lane 1 showing a middle range DNA ladder, lane 2 contains a 174 bp amplicon, and lane 3 showing the 1320 bp amplicon.[52]

they are both 24 nucleotides long and they differ by only one nucleotide. The one nucleotide difference in these probes did not affect the refractive index of the samples.

On the contrary, a difference in the transmitted light intensity was noticed after the addition of the target DNA in samples C+ and M+. These samples show transmitted light levels that are lower than those of samples R, C−, and M−, with sample C+ showing lowest transmitted light levels. The difference in the transmitted light intensities between samples C+ and M+ is attributed to the mismatch in probe M as it contained one different nucleotide in comparison to probe C. Therefore. These results demonstrate that when there are mismatches, the optical thickness will differ between the samples and the differences in optical thickness are directly linked with the sensor layer thickness.[31] Thus, the higher transmitted light intensity in the sample with probe M+ is attributed to incomplete binding between the probe and the target DNA. Furthermore, the addition of the target DNA to form a dsDNA with the probe caused a change in the refractive indices of samples C+ and M+, hence they exhibited a further reduction in transmitted light intensities. The differences in the transmitted light intensities observed in the samples that only had probes and those that had dsDNA due to the binding of the complementary probe to the target DNA align with what was observed by Elhaji et al. In that study, it was reported that the refractive index and percentage reflectivity of ssDNA is different from that of dsDNA. With dsDNA having $n = 1.53$ and ssDNA has $n = 1.46$.[30] Several studies have detected DNA mismatches using LSPR; Rapisarda et al.[37] used LSPR to study the hybridization process of perfectly matching and single base mismatching DNA using sensor chips with gold nanodisks and thiol - modified probes.[37] However, the current study used biotinylated probes on neutravidin-functionalized gold-coated surface. For the detection of p53 mutation, an amine terminated probe on a silver sensor chip was used and discriminated single base mutations in the p53 gene as they observed different shifts in peak of LSPR extinction spectra.[38] In another study, two tumor specific mutations E542K and E545K were successfully detected using thiolated peptide nucleic acid probes.[57] Despite the great work that has been achieved thus far, the ability of LSPR biosensors to detect small biological molecules remains limited. For a successful detection of small biological molecules, LSPR surface coating requires a large number of these biological molecules.[42] In addition, the biofouling of nanoparticle surfaces can also make it difficult to identify complex biological media, like urine and blood, thus affecting LSPR biosensing specificity.[43] Different strategies have been implemented to improve some of the LSPR challenges: the detection limits of small biological molecules are increased by changing the size, shape, and material of nanoparticles.[44] Plasmonic nanoparticle coupling-mediated amplification has been explored as the solution to the surface molecules, this approach includes an analyte-induced application for coupling of plasmons.[45] To improve selectivity in complex biological molecules, a DNA -ligated nanoparticle approach has been explored where a specific hybridization of a known target is attained.[46]

To confirm the binding of the biotinylated probe to avidin as well as the binding of the probe to the target DNA, DNA

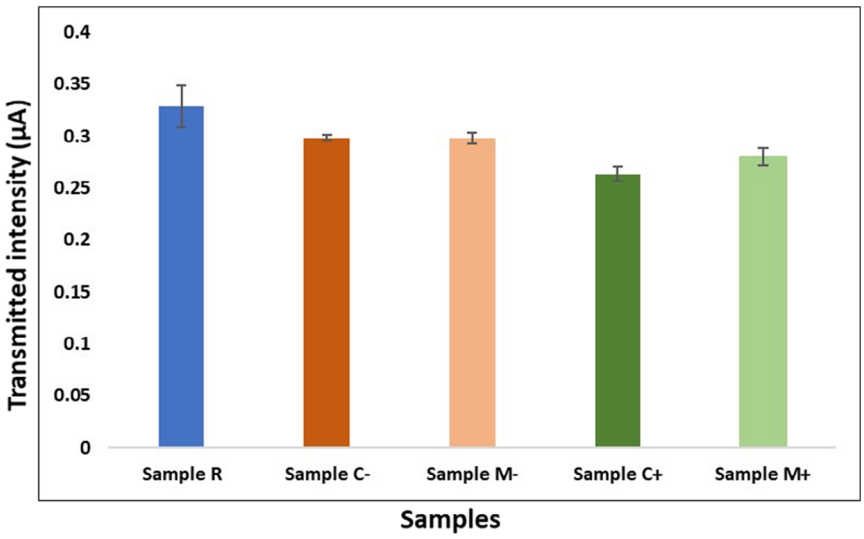

Figure 4. LSPR results displaying different transmitted light intensities of the five samples; sample R at 0.32 μA, samples C– and M– with 0.29 μA, sample C+ with 0.26 μA, and sample M+ showing 0.28 μA.

bioconjugation with streptavidin-functionalized AuNPs was performed and samples characterized using UV–vis spectroscopy, FTIR spectroscopy, DLS, and zeta potential. AuNPs were used because of their high surface to volume ratio, size flexibility, easy functionalization of their surface, and biocompatibility.[58] The UV–vis spectroscopy results of AuNPs only expressed as sample R (black curve) in **Figure 5** showed a prominent peak at 650 nm.

According to cytodiagnostics characterization of AuNPs, they strongly absorb light in the visible region between 500 and 700 nm when measured by UV–vis spectroscopy.[59] The absorbance wavelength peak varies depending on the particle diameter and shape, as such the uneven shaped particles like the nanourchins used in this study, their absorbance peak significantly shifts into the far-red area of the spectrum in comparison with the spherical particles of the same size. Furthermore, in functionalized nanoparticles (bound to a ligand), the spectrum redshifts more, which is why the nanourchins used here have a notable peak at 650 nm because they are functionalized with streptavidin.[59] Due to the binding of these AuNPs to streptavidin, they also have a peak between 260 and 280 nm, where nucleic acids and proteins absorb light, with 280 nm being the wavelength where most proteins including streptavidin absorb light.[60] The 650 nm absorbance intensity peak was not affected in samples C− and M− after the addition of probes in the nanoparticles. However, the 260/280 nm peak increases in these samples. In samples that had the probe and the target DNA (samples C+ and M+), the intensity at 260/280 nm is the highest due to the increase in DNA levels after the addition of the target DNA in the presence of a probe and the formation of dsDNA in the region where the probe binds to the target DNA. It was interesting to observe that the intensity peak at 650 nm in sample C+ is less than that of the sample M+, which could signify that the probe C was completely bound to the target DNA, whereas the binding with probe M was wobble due to the nucleotide mismatch. This result correlates with that of Murdock et al.[61]

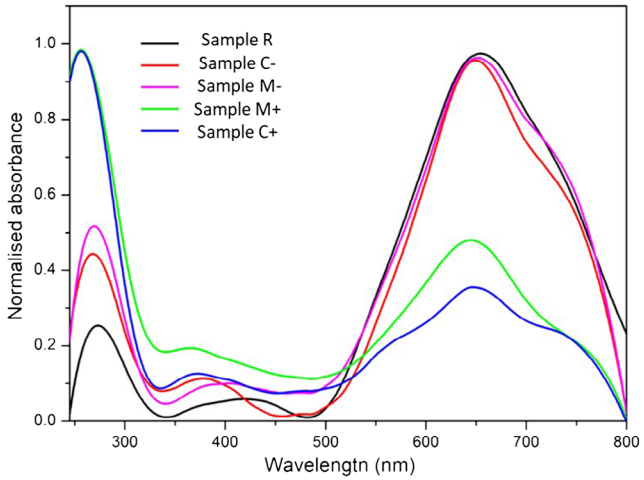

Figure 5. UV–vis spectroscopy results showing the gold nanoparticles absorbance peak at 650 nm and the DNA and protein absorbance peak at 260/280 nm. Gold nanoparticles bio-conjugated to DNA (samples C–, C+, M–, and M+) absorb more light in the 260/280 nm region and less light at 650 nm compared to sample R, the non-conjugated nanoparticles.

when the hybridization state of DNA-functionalized AuNPs was tested.[61]

The FTIR spectroscopy was used to identify functional groups present in the samples as summarized in **Table 2**. **Figure 6**A shows functional groups in streptavidin-functionalized AuNPs and Figure 6B shows functional groups present in streptavidin-functionalized nanoparticles conjugated to biotinylated DNA. Looking at the prominent peaks present in both samples, there is no notable difference. According to the chemical structures of the components in the compounds, the prominent peaks expected are shown in Table 2.

The vibration at 3354 cm^{-1} in Figure 6B represents the carbonic acid and the N–H stretch, it is assumed that the absorption peak is a combination due to the presence of water, as the samples were in liquid form and air dried. The peaks are not at the exact wavelengths from the prediction tables because a shift is often observed because of the reaction of more than one compound, which end up producing a new compound. The new produced compound is assumed to be the cause of this shift and the weak peak intensities.

The DLS technique in conjunction with the zeta potential surface charge measurements provides a broad range of information on nanobiosensor materials. This technique takes advantage of the Brownian motion of the particles that are dispersed in a solvent. The DLS size measurements are shown in **Figure 7** and **Table 3**. Here, it was observed that the average size of the streptavidin-functionalized AuNPs (Sample R) was 122 nm, ranging between 38 nm (0.14%) and 396 nm (0.09%) with 86% of particles falling within the range of 68–220 nm.

The addition of the biotinylated DNA probe to form sample C− increased the average size to 220 nm. The change in size equates to an increase of 98 nm, when comparing with sample R. This is indicative of the adsorption of the biotinylated DNA to the surface of the streptavidin-functionalized AuNPs.[62–64] A further increase slight increase of 25 nm, when comparing sample C− and sample C+. The slight size increase is indicative of the DNA probe binding to the target DNA rather than a formation of an adlayer.[63] These results give a strong indication that the DNA did bind to the nanoparticles and thereby confirming that the binding also took place in DNA hybridization on a gold-coated surface.

The zeta potential measurements are presented in Table 3. Here, it was observed that the zeta potential of the

Table 2. Functional groups and absorption wavenumbers.

Functional groups	Absorption wavenumbers [cm^{-1}]	Identification
COOH	3100–3400	Carboxylic acid stretch
C–H	2600–2850	Sp3 stretch
C=O	1640–1810	Carbonyl group
C–N	1250	Nitriles
N–H	3100–3500	secondary amide
P=O	1100–1200	Phosphates
S–H	2550–2600	Thiols
m-chlorobenzene	880–900	Meta-substituted benzene ring

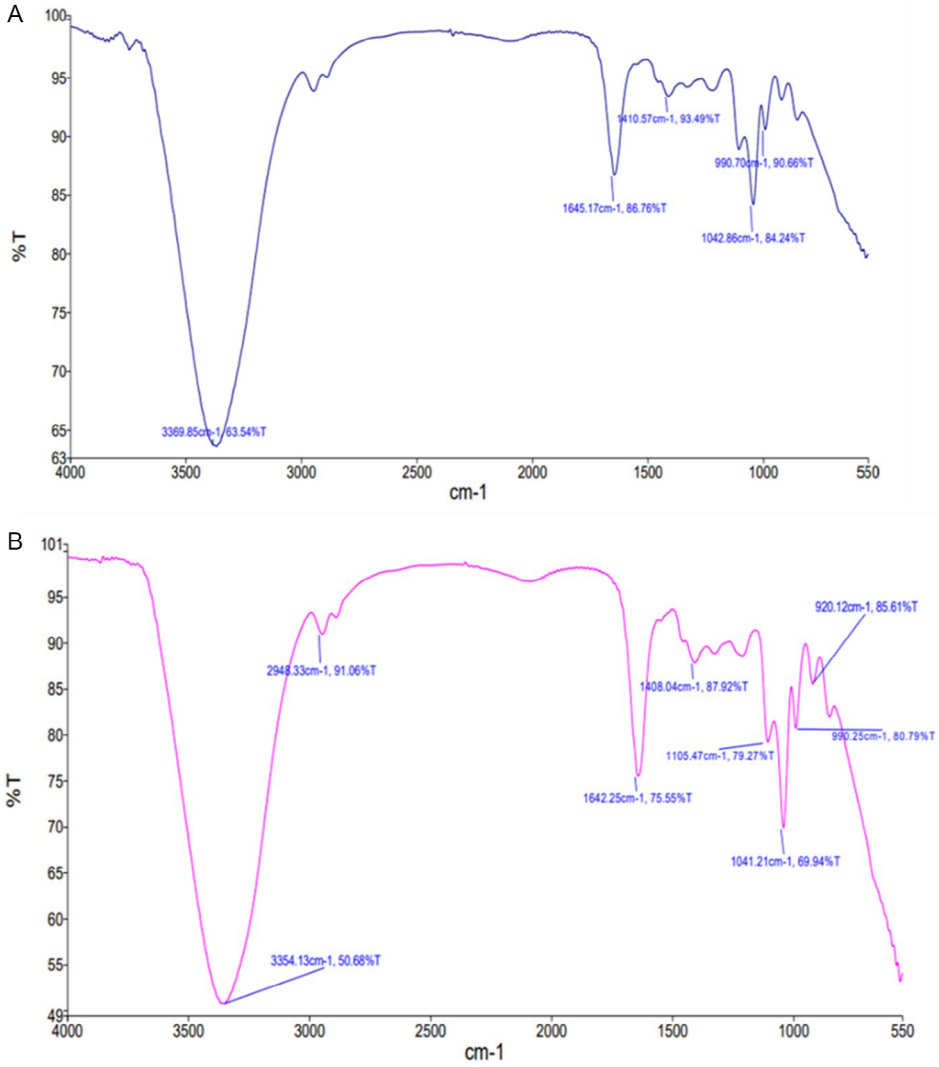

Figure 6. FTIR spectroscopy results: A) sample R that contains the streptavidin-functionalized gold nanoparticles and B) sample C+ which contains gold nanoparticles, biotinylated probe, and target DNA.

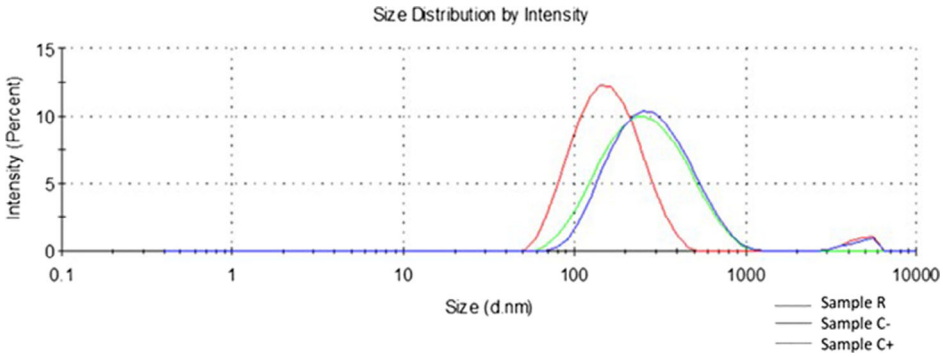

Figure 7. Gaussian curves representing the z-average size of the various materials.

streptavidin-functionalized AuNPs was −16.1 mV. This zeta potential was made to be more negative, −20.2, upon the formation of the biotinylated DNA layer on the functionalized AuNPs. The increase in the negativity of the sample C− is useful for the stabilization of the nanoparticles and the increased absorption of the biomolecules to the probe.[64] The binding

Table 3. Data DLS and zeta potential characterization of the various materials dispersed in water.

Sample	ζ [mV][a]	Z average [nm][b]	PDI[c]
Sample R	−16.1	122	0.236
Sample C–	−20.2	220	0.280
Sample C=	−17.2	255	0.259

[a]Zeta potential; [b]intensity-weighted harmonic mean hydrodynamic diameter; and [c]polydispersity index (PDI) from DLS measurements.

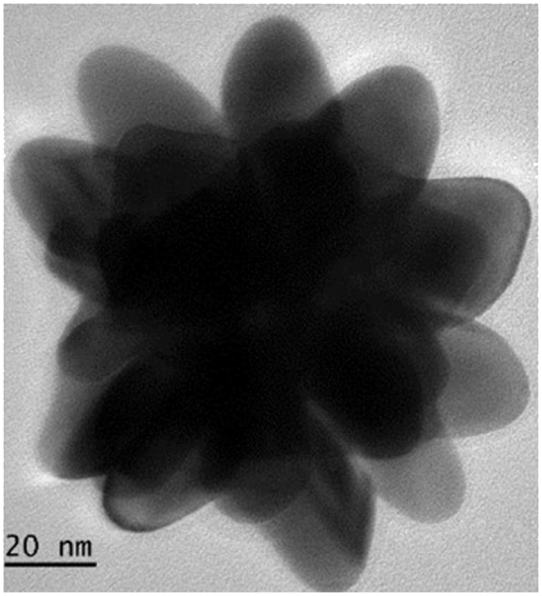

Figure 8. Transmission electron microscope image of gold nanourchins nanoparticles. The AuNPs were an average size of 90 nm and displayed a multibranched shape with a spiky uneven surface.

of the single target DNA molecule resulted in a slightly more positive material.

TEM image as shown in **Figure 8** confirmed that the AuNPs appeared predominantly multibranched with a spiky uneven surface, which is a typical characteristic of gold nanourchins.[65] The AuNPs had an average size of the 90 nm. The spikes found in this type of AuNPs causes a redshift in the surface plasmon peak and a larger enhancement of the electromagnetic field at the tips of the spikes compared to spherical nanoparticles.[66] According to the TEM results, the conjugation of DNA to the nanoparticles did not introduce physical and visible modification. This was as expected hence, chemical modifications were observed using UV/vis spectroscopy, DLS, zeta potential, and FTIR. TEM was meant to ensure that indeed the conjugation of DNA with nanoparticles did not alter the physical structure of the nanoparticle.

4. Conclusion

The LSPR optical biosensor presented here can detect DNA mismatches in DNA-hybridization experiments on gold-coated surfaces as demonstrated by differences in light intensities between the complementary and partial complementary probe. The possibility to detect DNA mismatches in this manner presents an opportunity to widen the technologies used in detecting DNA mismatches and mutations, which can be simpler to use at point-of-care settings. This technique will be explored in detecting HIV-drug-resistance mutations. Since the current work focused on detecting DNA mismatches, more work is still required to determine optimal conditions of LSPR biosensing for detecting DNA mismatches when using the biotin – neutravidin approach. The parameters to be investigated include neutravidin concentration for functionalizing the sensor chip, the concentration, the length of both the probe and the target DNA, as well as sample preparation when detecting mutations in biological specimens such as blood and sputum. Furthermore, temperature and pH will also be evaluated as temperature fluctuations have been reported to have notable effects on some plasmonic biosensors.[67]

Acknowledgements

This work was financially supported by the Council for Scientific and Industrial Research, Department of Science and Innovation of South Africa as well as the Africa Laser Centre. This research was scientifically supported by Sello Manoto, Charles Maphanga, and the CSIR Nanotechnology Centre.

Conflict of Interest

The authors declare no conflict of interest.

Data Availability Statement

Research data are not shared.

Keywords

deoxyribonucleic acid, localized surface plasmon resonances, mismatches, mutations, optical biosensors

Received: October 4, 2023
Revised: March 15, 2024
Published online: May 15, 2024

[1] E. Chargaff, *Experientia* **1950**, *6*, 201.
[2] J. D. Watson, F. H. C. Crick, *Nature* **1953**, *171*, 964.
[3] C. Molnar, J. Gair, *Concepts of Biology* **2015**.
[4] B. Alberts, A. Johnson, J. Lewis, *Molecular Biology of the Cell*, 4th ed, Garland, New York **2002**.
[5] F. H. C. Crick, *J. Mol. Biol.* **1966**, *19*, 548.
[6] J. T. Stivers, Y. L. Jiang, *Chem. Rev.* **2003**, *103*, 2729.
[7] G.-M. Li, *Cell Res.* **2008**, *18*, 85.
[8] M. S. Smolinski, M. A. Hamburg, J. Lederberg, *Microbial Threats to Health: Emergence, Detection, and Response*, National Academies Press, Washington, DC **2003**.
[9] S. Mummidi, S. S. Ahuja, E. Gonalez, S. A. Anderson, E. N. Santiago, K. T. Stephan, F. E. Craig, P. O'connell, V. Tryon, R. A. Clark, M. J. Dolan, S. K. Ahuja, *Nat. Med.* **1998**, *4*, 786.

[10] Cystic Fibrosis - What is Cystic Fibrosis? **2022** www.nhlbi.nih.gov (accessed: May 2023).
[11] W. M. Howell, M. Jobs, U. Gyllensten, A. J. Brookes, *Nat. Biotechnol.* **1999**, *17*, 87.
[12] C. R. Newton, A. Graham, L. E. Heptinstall, S. J. Powell, C. Summers, N. Kalsheker, J. C. Smith, A. F. Markham, *Nucleic Acids Res.* **1989**, *17*, 2503.
[13] R. W. Peeling, K. K. Holmes, D. Mabey, A. Ronald, *Sex. Transm. Infect.* **2006**, *82*, v1.
[14] V. Gubala, L. F. Harris, A. J. Ricco, M. X. Tan, D. E. Williams, *Anal. Chem.* **2012**, *84*, 487.
[15] A. Skrahina, H. Hurevich, A. Zalutskaya, E. Sahalchyk, A. Astrauko, W. Van Gemert, S. Hoffner, V. Rusovich, M. Zignol, *Eur. Respir. J.* **2012**, *39*, 1425.
[16] D. Pillay, A. Walker, D. Gibb, A. De Rossi, S. Kaye, M. Ait-Khaled, M. Muñoz-Fernandez, A. Babiker, *J. Infect. Dis.* **2002**, *186*, 617.
[17] P. Estrela, P. Damborský, J. Švitel, J. Katrlík, *Essays Biochem.* **2016**, *60*, 91.
[18] M. Aizawa, K. Nishiguchi, M. Imamura, E. Kobatake, T. Haruyama, Y. Ikariyama, *Sens. Actuators, B* **1995**, *24*, 1.
[19] J. J. Ramsden, *J. Mol. Recognit.* **1997**, *10*, 109.
[20] K. M. Mayer, J. H. Hafner, *Chem. Rev.* **2011**, *111*, 3828.
[21] J. M. Brockman, B. P. Nelson, R. M. Corn, *Annu. Rev. Phys. Chem.* **2000**, *51*, 41.
[22] A. J. Haes, R. P. Van Duyne, *J. Am. Chem. Soc.* **2002**, *124*, 10596.
[23] H. Zhang, X. Zhou, X. Li, P. Gong, Y. Zhang, Y. Zhao, *Biosensors* **2023**, *13*, 405.
[24] C. R. Basso, T. F. Cruz, B. L. Silva, V. A. Pedrosa, J. P. Araújo Junior, *Materials* **2020**, *13*, 1087.
[25] W. Wang, Y. You, S. Gunasekaran, *Compr. Rev. Food Sci. Food Saf.* **2021**, *20*, 5829.
[26] M. Manzano, P. Vizzini, K. Jia, P.-M. Adam, R. E. Ionescu, *Sens. Actuators, B* **2016**, *223*, 295.
[27] J. Hu, K. Fu, P. W. Bohn, *Anal. Chem.* **2018**, *90*, 2326.
[28] O. Adegoke, M. Morita, T. Kato, M. Ito, T. Suzuki, E. Y. Park, *Biosens. Bioelectron.* **2017**, *94*, 513.
[29] X. Wang, Y. Li, H. Wang, Q. Fu, J. Peng, Y. Wang, J. Du, Y. Zhou, L. Zhan, *Biosens. Bioelectron.* **2010**, *26*, 404.
[30] K. Takemura, O. Adegoke, N. Takahashi, T. Kato, T.-C. Li, N. Kitamoto, T. Tanaka, T. Suzuki, E. Y. Park, *Biosens. Bioelectron.* **2017**, *89*, 998.
[31] W. Sun, S. Yuan, H. Huang, N. Liu, Y. Tan, *J. Microbiol. Methods* **2017**, *142*, 41.
[32] A. Taghipour, H. Heidarzadeh, *Photonics* **2022**, *9*, 542.
[33] M. Bhagawati, C. You, J. Piehler, *Anal. Chem.* **2013**, *85*, 9564.
[34] M. Cottat, N. Thioune, A.-M. Gabudean, N. Lidgi-Guigui, M. Focsan, S. Astilean, M. Lamy De La Chapelle, *Plasmonics* **2013**, *8*, 699.
[35] J. Roether, K.-Y. Chu, N. Willenbacher, A. Q. Shen, N. Bhalla, *Biosens. Bioelectron.* **2019**, *142*, 111528.
[36] X. Qi, J. Bi, *Opt. Commun.* **2019**, *453*, 124328.
[37] A. Rapisarda, N. Giamblanco, G. Marletta, *J. Colloid Interface Sci.* **2017**, *487*, 141.
[38] R. Q. Duan, J. L. Yuan, H. Yang, X. G. Luo, M. R. Xi, *Neoplasma* **2012**, *59*, 348.
[39] J.-S. Chen, P.-F. Chen, H. T.-H. Lin, N.-T. Huang, *Analyst* **2020**, *145*, 7654.
[40] J. Cao, E. K. Galbraith, T. Sun, K. T. V. Grattan, *J. Phys. Conf. Ser.* **2011**, *307*, 012050.
[41] S. S. Aćimović, H. Šípová, G. Emilsson, A. B. Dahlin, T. J. Antosiewicz, M. Käll, *Light: Sci. Appl.* **2017**, *6* e17042.
[42] A. B. Dahlin, *Sensors* **2012**, *12*, 3018.
[43] O. Kedem, A. Vaskevich, I. Rubinstein, *J. Phys. Chem. C* **2014**, *118*, 8227.
[44] J. C. Sharpe, J. S. Mitchell, L. Lin, N. Sedoglavich, R. J. Blaikie, *Anal. Chem.* **2008**, *80*, 2244.
[45] A. Pandya, P. G. Sutariya, S. K. Menon, *Analyst* **2013**, *138*, 2483.
[46] F. Xia, X. Zuo, R. Yang, Y. Xiao, D. Kang, A. Vallée-Bélisle, X. Gong, J. D. Yuen, B. B. Y. Hsu, A. J. Heeger, K. W. Plaxco, *Proc. Natl. Acad. Sci.* **2010**, *107*, 10837.
[47] H. Nguyen, J. Park, S. Kang, M. Kim, *Sensors* **2015**, *15*, 10481.
[48] J. Homola, S. S. Yee, G. Gauglitz, *Sens. Actuators, B* **1999**, *54*, 3.
[49] C. Maphanga, S. Manoto, S. Ombinda-Lemboumba, Y. Ismail, P. Mthunzi-Kufa, *Sens. Bio-Sens. Res.* **2023**, *39*, 100545.
[50] C. Maphanga, S. Manoto, S. Ombinda-Lemboumba, Y. Ismail, P. Mthunzi-Kufa, *Proc. SPIE* **2023**, *12387*, 123870E.
[51] U.S. National Library of Medicine, Basic Local Alignment Search Tool, https://blast.ncbi.nlm.nih.gov/Blast.cgi (accessed: January 2021).
[52] M. Y. Lugongolo, S. L. Manoto, C. Maphanga, S. Ombinda-Lemboumba, S. L. Thobakgale, P. Mthunzi-Kufa, *Proc. SPIE* **2021**, *11661*, 116610M.
[53] E. P. Diamandis, T. K. Christopoulos, *Clin. Chem.* **1991**, *37*, 625.
[54] I. Mannelli, M. Minunni, S. Tombelli, R. Wang, M. Michela Spiriti, M. Mascini, *Bioelectrochemistry* **2005**, *66*, 129.
[55] S. Elhadj, G. Singh, R. F. Saraf, *Langmuir* **2004**, *20*, 5539.
[56] Q.-Q. Wu, K.-G. Wang, D. Sun, S. Wang, C. Zhang, W. Zhao, *Chin. Phys. Lett.* **2016**, *33*, 088701.
[57] A. H. Nguyen, S. J. Sim, *Biosens. Bioelectron.* **2015**, *67*, 443.
[58] R. R. Arvizo, S. Bhattacharyya, R. A. Kudgus, K. Giri, R. Bhattacharya, P. Mukherjee, *Chem. Soc. Rev.* **2012**, *41*, 2943.
[59] Introduction to Gold Nanoparticle Characterization **2023**, https://www.cytodiagnostics.com/pages/introduction-to-gold-nanoparticle-characterization (accessed: June 2023).
[60] H. Edelhoch, *Biochemistry* **1967**, *6*, 1948.
[61] R. C. Murdock, O. A. Khan, T. J. Lamkin, S. M. Hussain, N. Kelley-Loughnane, *Int. J. Opt.* **2017**, *2017*, 8427459.
[62] R. D'Agata, P. Palladino, G. Spoto, *Beilstein J. Nanotechnol.* **2017**, *8*, 1.
[63] W. Eimer, J. R. Williamson, S. G. Boxer, R. Pecora, *Biochemistry* **1990**, *29*, 799.
[64] S. Park, K. A. Brown, K. Hamad-Schifferli, *Nano Lett.* **2004**, *4*, 1925.
[65] C. Kohout, C. Santi, L. Polito, *Int. J. Mol. Sci.* **2018**, *19*, 3385.
[66] M. Falahati, F. Attar, M. Sharifi, A. A. Saboury, A. Salihi, F. M. Aziz, I. Kostova, C. Burda, P. Priecel, J. A. Lopez-Sanchez, S. Laurent, N. Hooshman, d, M. A. El-Sayed, *Biochim. Biophys. Acta, Gen. Subj.* **2020**, *1864*, 129435.
[67] C.-V. Topor, M. Puiu, C. Bala, *Biosensors* **2023**, *13*, 465.